Contents lists available at ScienceDirect

Acta Biomaterialia

journal homepage: www.elsevier.com/locate/actbio



Full length article

Regional and disease-specific glycosaminoglycan composition and function in decellularized human lung extracellular matrix



Evan Hoffman^a, Yuefan Song^b, Fuming Zhang^b, Loredana Asarian^a, Isaac Downs^a, Brad Young^a, Xiaorui Han^b, Yilan Ouyang^b, Ke Xia^b, Robert J. Linhardt^b, Daniel J. Weiss^{a,*}

^a Larner College of Medicine, University of Vermont, 149 Beaumont Avenue, Health Science Research Facility (HSRF) 226, Burlington, VT 05405, USA

ARTICLE INFO

Article history: Received 24 February 2023 Revised 16 June 2023 Accepted 28 June 2023 Available online 9 July 2023

Keywords: Lung Decellularization Glycosaminoglycan Matrix-associated growth factors Extracellular matrix gel

ABSTRACT

Decellularized lung scaffolds and hydrogels are increasingly being utilized in ex vivo lung bioengineering. However, the lung is a regionally heterogenous organ with proximal and distal airway and vascular compartments of different structures and functions that may be altered as part of disease pathogenesis. We previously described decellularized normal whole human lung extracellular matrix (ECM) glycosaminoglycan (GAG) composition and functional ability to bind matrix-associated growth factors. We now determine differential GAG composition and function in airway, vascular, and alveolar-enriched regions of decellularized lungs obtained from normal, chronic obstructive pulmonary disease (COPD), and idiopathic pulmonary fibrosis (IPF) patients. Significant differences were observed in heparan sulfate (HS), chondroitin sulfate (CS), and hyaluronic acid (HA) content and CS/HS compositions between both different lung regions and between normal and diseased lungs. Surface plasmon resonance demonstrated that HS and CS from decellularized normal and COPD lungs similarly bound fibroblast growth factor 2, but that binding was decreased in decellularized IPF lungs. Binding of transforming growth factor β to CS was similar in all three groups but binding to HS was decreased in IPF compared to normal and COPD lungs. In addition, cytokines dissociate faster from the IPF GAGs than their counterparts. The differences in cytokine binding features of IPF GAGs may result from different disaccharide compositions. The purified HS from IPF lung is less sulfated than that from other lungs, and the CS from IPF contains more 6-0-sulfated disaccharide. These observations provide further information for understanding functional roles of ECM GAGs in lung function and disease.

Statement of significance

Lung transplantation remains limited due to donor organ availability and need for life-long immunosuppressive medication. One solution, the ex vivo bioengineering of lungs via de- and recellularization has not yet led to a fully functional organ. Notably, the role of glycosaminoglycans (GAGs) remaining in decellularized lung scaffolds is poorly understood despite their important effects on cell behaviors. We have previously investigated residual GAG content of native and decellularized lungs and their respective functionality, and role during scaffold recellularization. We now present a detailed characterization of GAG and GAG chain content and function in different anatomical regions of normal diseased human lungs. These are novel and important observations that further expand knowledge about functional GAG roles in lung biology and disease.

© 2023 The Authors. Published by Elsevier Ltd on behalf of Acta Materialia Inc. This is an open access article under the CC BY-NC-ND license (http://creativecommons.org/licenses/by-nc-nd/4.0/)

1. Introduction

Decellularized lungs and materials derived from these, including hydrogels and bioinks, are increasingly being utilized in studies of lung regenerative engineering. These are important tools that

^b Rensselaer Polytechnic Institute, Center for Biotechnology and Interdisciplinary Studies, Troy, NY, USA

Corresponding author. E-mail address: daniel.weiss@uvm.edu (D.J. Weiss).

allow sophisticated study of the influence of the extracellular matrix (ECM) on cell behaviors. Accordingly, it is important to understand regional and disease-related variation in ECM proteins as well as glycosaminoglycans (GAGs) and proteoglycans (PGs) remaining in the decellularized lungs [1–3]. As demonstrated by a number of groups, GAGs in particular play important roles in ECM homeostasis and normal repair processes and help direct ECM assembly, organization, and remodeling during [4,5]. GAGs further facilitate cell-ECM interactions by direct interaction with cell membrane receptors, sequestration and presentation of bioactive molecules such as growth factors, and as anchor sites for cells to recognize or attach to the local ECM architecture [6–10]. Further, lung ECM GAGs significantly affect behavior and proper functioning of the cells seeded directly into the decellularized lungs or into derivative gels produced from them [11–13].

The lung is a heterogenous organ, with structural and ECM compositional differences between anatomical regions which critically contribute to different regional functions. Further, as demonstrated by us and others, ECM GAG content and distribution can be significantly altered in lung diseases such as chronic obstructive pulmonary disease (COPD) and idiopathic pulmonary fibrosis (IPF) [2,11,12]. However, the regional GAG content, distribution, and function in decellularized normal as well as COPD and IPF lungs remains poorly understood. Better understanding of this will provide further insights into lung disease pathogenesis and provide potential new therapeutic approaches.

We have previously systematically assessed GAG content and function in whole decellularized human lungs obtained from autopsy [2]. This included lungs from patients with no history or clinical evidence of lung disease as well as lungs from patients with documented COPD. We have also recently profiled the ECM protein composition in the airways, alveolar-enriched regions, and vasculature of decellularized normal, COPD, and IPF lungs and have found notable differences between both regions and between normal and diseased lungs [14]. We have now analyzed materials obtained from these same lungs to better understand the distribution of ECM GAGs in different anatomical regions and to further assess disease-related changes in distribution and function. Significant differences in content and distribution of major GAGs as well as in specific disaccharide composition in these classes were observed between different anatomic regions and between normal and diseased lungs, particularly IPF lungs. Surface plasmon resonance (SPR) demonstrated significant differences in ability of HS and CS in IPF lungs to bind fibroblast growth factor 2 (FGF2) and of HS to bind transforming growth factor β (TGF β 1) compared to normal and COPD lungs. These data further define the roles of ECM GAGs in lung biology and disease and offer new mechanistic studies and potential therapeutic avenues.

2. Materials and methods

2.1. Human lungs

Human lungs were obtained from the University of Vermont (UVM) autopsy services under appropriate institutional guidelines. Lungs were categorized into those from lifelong non-smokers, former or current smokers, patients with clinical and/or radiographic COPD, or patients with clinical and/or idiopathic pulmonary fibrosis based on available medical records. These same lungs have been previously analyzed by mass spectrometry for determination of protein composition [14].

2.2. Reagents

Unsaturated disaccharide standards of CS (Δ UA-GalNAc; Δ UA-GalNAc4S; Δ UA-GalNAc6S; Δ UA2S-GalNAc; Δ UA2S-Gal-NAc4S;

ΔUA2S-GalNAc6S; ΔUA-GalNAc4S6S; ΔUA2S-GalNAc4S6S), unsaturated disaccharide standards of HS (ΔUA-GlcNAc; ΔUA-GlcNS; ΔUA-GlcNAc6S; ΔUA2S-GlcNAc; ΔUA2S-GlcNS; ΔUA-GlcNS6S; ΔUA2S-GlcNAc6S; ΔUA2S-GlcNS6S), and unsaturated disaccharide standard of HA (Δ UA-GlcNAc), where Δ UA is 4-deoxy- α -L-threohex-4-enopyranosyluronic acid, were purchased from Iduron (UK). Actinase E was obtained from Kaken Biochemicals (Japan). Chondroitin lyase ABC from Proteus vulgaris was expressed in our laboratory. Recombinant Flavobacterial heparin lyases I, II, and III were expressed in our laboratory using Escherichia coli strains provided by Jian Liu (College of Pharmacy, University of North Carolina). 2-Aminoacridone (AMAC), sodium cyanoborohydride were obtained from Sigma-Aldrich (St. Louis, MO, USA). All solvents were HPLC grade. FGF2, recombinant human TGF β 1 were obtained from R&D Systems, Bio-Techne. Actinase E was obtained from Kaken Biochemicals (Japan). Chondroitin lyase ABC from Proteus vulgaris was expressed in our laboratory. Recombinant Flavobacterial heparin lyases I, II, and III were expressed in our laboratory using E. coli strains provided by Jian Liu (College of Pharmacy, University of North Carolina). Sensor SA chips were from GE Healthcare (Uppsala, Sweden).

2.3. Decellularization

Human lungs were decellularized using a combined perfusion and physical approach we have developed [15,16]. Individual lobes were separated from one another prior to decellularization. Decellularization fluids were instilled at a flow rate of 2 L/min which we have determined to maximize instillation of decellularization fluids and minimize tissue damage [15]. On day 1 of the decellularization protocol, the lungs are rinsed with 8 L of de-ionized (DI) water containing 500 IU/mL Penicillin/500 µg/mL Streptomycin (5X pen/strep) (Lonza) through both the lobar main stem bronchus and the major vascular arterial supplies to each respective lobe. Next, 4L of 0.1% Triton-X (Sigma) and 5X pen/strep in DI water is infused through airway and vascular ports. Lobes are submerged in Triton-X solution and incubated on a shaker table for 24 h at 4°C. On day 2, the lungs are removed from Triton-X and rinsed with 8L of DI water and 5X pen/strep as previously described. Four liters of 2% sodium deoxycholate (SDC, Sigma) and 100 IU/mL Penicillin/100 μ g/mL Streptomycin (1X pen/strep) in DI water was then instilled as previously described for day 1. Lungs are incubated in SDC and placed on a shaker table for 24 h at 4°C. The next day, lungs are removed from the SDC solution and rinsed with 8L of DI water and pen/strep. 4 L of 1 M NaCl (USB) and 5X pen/strep in DI water is instilled into the lung. The lungs are then incubated in the NaCl solution and placed on a shaker table for 1 h at room temperature (~25°C). Lungs are removed from the NaCl solution, rinsed with 8 L of DI water and penstrep, and then instilled with 4 L of 30 μg/mL porcine pancreatic DNase (Sigma), 2 mM CaCl₂ (Sigma), 1.3 mM MgSO₄ (Sigma), and 5X pen/strep in DI water and incubated on a shaker table for 1 h at room temperature. The lungs are removed from the DNase solution, rinsed with 8 L of DI water and pen/strep, and then infused with 4 L of 0.1% peracetic acid (Sigma) in 4% ethanol solution and incubated on a shaker table for 2 h at room temperature. Finally, lungs are removed from the peracetic acid solution and rinsed with 12-15 L of a 5X pen/strep, 50 mg/L gentamicin (Cellgro), 2.5 μ g/mL Amphotericin B (Cellgro) in 1X PBS solution (storage solution) as described for the pen/strep DI water rinses. Lungs are stored in storage solution at 4°C until needed.

Decellularization efficiency is assessed by measurement of residual double-stranded DNA (dsDNA) and by hematoxylin and eosin (H&E) staining, as previously described [14–16]. In brief, native and decellularized lung fragments (\sim 1 mm³) are excised from the distal portion of the lung, fixed in 4% paraformaldehyde, and mounted as 5 µm sections for H&E staining. Quantitative dsDNA

quantification of lyophilized native and decellularized lung samples is performed using DNeasy Blood & Tissue Kit (Qiagen) and QuantiT PicoGreen dsDNA Assay Kit (Thermo) according to the manufacturer's protocols. Qualitative assessment of any potential residual dsDNA is performed by gel electrophoresis on an 0.8% agarose gel labelled with STBR Safe DNA Gel stain (Thermo) [15,16].

For preparing regional anatomic samples, whole decellularized lung lobes were manually dissected to remove airway and vasculature trees. Surgical scissors and forceps were used to expose the most proximal regions of the airways, which were subsequently used as a guide to carefully dissect down the length of the airways towards the most distal tips of airway trees. As expected, decellularized vascular tissue remained in close proximity to the airway regions during the dissection process, yet differed in color and elasticity, making it simple to identify and remove from the airway. Airway samples between \sim 1-5 mm were taken for further processing (~airway generations 2-16) [14]. Alveolar-enriched tissue was identified as the distal tips of the small branching airways < 1 mm (~airway generations 17-23). Isolated samples were grouped as whole lung (i.e., non-dissected fractions obtained from the ventral portion of the lung and containing all regions), airways, vasculature, or alveolar-enriched regions. Samples from the individual lungs were frozen at -80°C, lyophilized, and liquid nitrogen milled (Freezer Mill, Spex) to a fine powder. The ECM powders were designated bulk (whole) lung ECM (wECM), airway ECM (airECM), vasculature ECM (vECM), or alveolar-enriched ECM (aECM) and stored at -20°C until future use.

2.4. Characterization of specific anionic GAGs and disaccharide composition in decellularized lungs

Decellularized lung tissue powders were proteolyzed at 55 °C with 20-mg/mL actinase E (total amount of actinase E: sample (w/w) = 0.8:1) for 24 h and followed by actinase E deactivation at 100 °C for 30 min. The volume of the above solution was recorded for each sample, and the amount of solution containing 1 mg of sample was transferred to a 10-kDa molecular weight cut off (MWCO) spin tube. Equal volume of 4% aqueous CHAPS solution was added and mixed with the solution in the filter of the spin tube. The filter unit was washed three times with 400 μ L distilled water and then added with 300-µL digestion buffer (50 mM NH₄HCO₃ containing 2 mM CaCl₂ adjusted to pH 7.0). Recombinant heparin lyase I, II, III (pH optima 7.0-7.5) and recombinant chondroitin lyase ABC (pH optimum 7.4, 10 mU each) were added to each filter unit containing sample and mixed well. The samples were all incubated at 37°C for 24 h. The enzymatic digestion was terminated by ultrafiltration through the 10-kDa spin tube. The filtrate was collected, and the filter unit was washed twice with 200 μ L distilled water. All the filtrates containing the disaccharide products were combined and dried via freeze dry. The liquid samples were washed three times with 400 μ L distilled water in 10-kDa spin tube, and then digested as mentioned above [17,18] The dried samples were AMAC-labeled by adding 10 μ L of 0.1 M AMAC in dimethyl sulfoxide/acetic acid (17/3, v/v) incubating at room temperature for 10 min, followed by adding 10 μ L of 1 M aqueous sodium cyanoborohydride and incubating for 1 h at 45°C. A mixture containing all 17-disaccharide standards prepared at 0.5 $ng/\mu L$ was similarly AMAC-labeled and used for each run as an external standard. After the AMAC-labeling reaction, the samples were centrifuged, and each supernatant was recovered.

Liquid chromatography-mass spectrometry (LC-MS) was performed on an Agilent 1200 LC system at 45°C using an Agilent Poroshell 120 ECC18 (2.7 $\mu m, 3.0 \times 50$ mm) column. Mobile phase A (MPA) was 50 mM ammonium acetate aqueous solution, and the mobile phase B (MPB) was methanol. The mobile phase passed through the column at a flow rate of 300 $\mu L/min$. The gradient was

0-10 min, 5-45% B; 10-10.2 min, 45-100%B; 10.2-14 min, 100% B; 14-22 min, 100-5% B. Injection volume is 5 μ L. A triple quadrupole mass spectrometry system equipped with an ESI source (Thermo Fisher Scientific, San Jose, CA) was used a detector. The online MS analysis was at the Multiple Reaction Monitoring (MRM) mode. MS parameters: negative ionization mode with a spray voltage of 3000 V, a vaporizer temperature of 300°C, and a capillary temperature of 270°C.

2.5. Purification of lung GAGs and binding of representative matrix-associated growth factors by competitive interaction using SPR

For the SPR analyses, two additional normal and COPD lungs were processed (Table 1B). HS or CS from normal or COPD samples was prepared from 250 mg of combined dried tissue powder. For IPF samples, 350 mg dried tissue powder of the same lungs utilized for the above studies was used for either HS or CS preparation. Powder samples were proteolyzed at 55°C with 20-mg/mL actinase E (total amount of actinase E: sample (w/w) = 0.8:1) for 24 h and followed by actinase E deactivation at 100°C for 30 min and then centrifuged at 4000 x g for 30 min. The supernatant was transferred into a 10-kDa molecular weight cut off (MWCO) spin tube and concentrated through centrifugation. The concentrated solution was recovered from the filter. Nine times volume of acetone was added to the solution to precipitate the glycans. The precipitates were further dissolved in H2O and washed through ultrafiltration using spin filters. For the HS preparation, the recombinant chondroitin lyase ABC (pH optimum 7.4, 2 U each) were added to each filter. For the CS preparation, recombinant heparin lyase I, II, III (pH optima 7.0-7.5, 2 U each) were added to each filter unit containing sample and mixed well. The samples were all incubated at 37°C for 24 h. The enzymatic digestion was terminated by ultrafiltration through the 10-kDa spin tube. The crude GAG was recovered from the filter and lyophilized. The lyophilized samples were dissolved in 400 µL of a solution of denaturing buffer (8 M urea containing 2% wt. 3[(3- cholamidopropyl)dimethylammonio]-1-propanesulfonate (CHAPS)), bound to Vivapure Q Mini H spin column, washed twice with 400 µL of denaturing buffer and washed three times with 400 μL of 0.2 M NaCl. The GAG components were then eluted from the spin column with three 400 μL volumes of 16% NaCl. The released GAGs are collected by ultrafiltration through a 10-kDa molecular weight cut off (MWCO) spin tube. The filter unit was washed twice with 400 μ L of distilled water to remove salt. The GAGs were collected from the filter unit and lyophilized. The purified HS and CS were subjected to dp2 analysis as mentioned above.

The purified HS and CS from different kinds of lung samples was biotinylated by conjugating to amine-PEG3-Biotin (Pierce, Rockford, IL). In brief, 0.5 mg of HS/CS and amine-PEG3-Biotin (0.5 mg, Pierce, Rockford, IL) were dissolved in 100 µL H₂O, 2.5 mg NaCNBH3 was added. The reaction mixture was heated at 70°C for 24 h, after that a further 2.5 mg NaCNBH3 was added, and the reaction was heated at 70°C for another 24 h. After cooling to room temperature, the mixture was desalted with the spin column (3,000 MWCO). Biotinylated GAGs were collected, freeze-dried, and used for SA chip preparation. The biotinylated GAGs were immobilized to streptavidin (SA) chip based on the manufacturer's protocol. The successful immobilization of heparin was confirmed by the observation of a >200 resonance unit (RU) increase on the sensor chip. The control flow cell (FC1) was prepared by 1 min injection with saturated biotin. The commercial heparin was biotinylated and immobilized in the same way as HS and CS and serve as reference.

Protein samples were diluted in HBS-EP buffer (0.01 M 4-(2-hydroxyethyl)-1-piperazineethanesulfonic acid (HEPES), 0.15 M NaCl, 3 mM ethylenediaminetetraacetic acid (EDTA), 0.005% sur-

Table 1ALungs utilized for GAG compositional analyses.

| Patient ID | Lung Designation | Age | Sex | Pulmonary History | Smoking History |
|----------------------------|------------------|-----|-----|---|---|
| ND1 | Non-diseased | 42 | M | None | Ex-smoker, quit 4 years prior to death |
| ND2 | Non-diseased | 73 | M | None | Ex-smoker, quit 49 years prior to death |
| ND3 | Non-diseased | 80 | M | None | Ex-smoker, quit 36 years prior to death |
| ND4 | Non-diseased | 64 | F | None | Ex-smoker, quit 20 years prior to death |
| ND5 | Non-diseased | 60 | F | None | Lifelong non-smoker |
| ND6 | Non-diseased | 84 | F | Acute lobar pneumonia at time of death (non-involved lobe used) | Lifelong non-smoker |
| COPD1 | COPD | 75 | M | Centroacinar emphysema | Ex-smoker, quit 36 years prior to death |
| COPD2 | COPD | 61 | M | Respiratory bronchiolitis on chest CT | Ex-smoker, quit 2 years prior to death |
| COPD3 | COPD | 57 | M | Centroacinar emphysema | Current smoker, 1 pack per day |
| IPF1 | IPF | 79 | M | Acute IPF exacerbation; Unclassified interstitial fibrosis; Areas of honeycombing | Ex-smoker, quit 27 years prior to death |
| IPF2 | IPF | 84 | M | Acute IPF exacerbation; Usual interstitial pneumonia (UIP) and honeycombing | Lifelong non-smoker |
| IPF3 | IPF | 67 | M | Hypoxic respiratory failure; Usual interstitial pneumonia and honeycombing | Ex-smoker, quit 49 years prior to death |
| IPF4 | IPF | 652 | F | Usual interstitial pneumonia (UIP) | Ex-smoker, quit 33 years prior to death |
| Patient Condition | | | | Mean Age | St. Dev. Age |
| Non-Diseased/Remote Smoker | | | | 62.25 | 16.21948 |
| COPD | | | | 60 | 12.08305 |
| IPF | | | | 73.75 | 9.215024 |

factant P20, pH 7.4,) to measure interaction between GAGs and cytokine using SPR [2,19]. Different dilutions of protein samples were injected at a flow rate of 30 μ L/min. At the end of the sample injection, the same buffer was flowed over the sensor surface to facilitate dissociation. After a 3 min dissociation time, the sensor surface was regenerated by injecting with 30 μ L of 2 M NaCl to get a fully regenerated surface. The response was monitored as a function of time (sensorgram) at 25°C. The kinetics was calculated using Biacore T200 Evaluation Software 3.2.

2.6. Statistical analyses

Data is displayed as mean \pm standard deviation (SD) or box plots with whiskers (Tukey). GAG quantification data is shown as paired plots matching native and decellularized tissue from each lung. The analytical variability for GAG disaccharide analysis is <3% [17,18]. Comparison between control and experimental conditions was done by one sample t-test against a fixed value, Students' t-test, or Two-way ANOVA with post-hoc Tukey's multiple comparisons test. Results were considered significant at p<0.05.

3. Results

For the lungs obtained at autopsy, individual patient demographics are depicted in **Table 1.** Data from **Table 1A** has been previously presented as supplemental information in a manuscript describing proteomic analyses of these same lungs [14]. IPF patients were older than either those with normal/remote smoking patients or those with COPD (74 \pm 9, 62 \pm 16 and 60 \pm 12, respectively). The normal/remote smoking group was 62.5% female with COPD and IPF groups at 100% and 75% male, respectively.

3.1. GAG composition varies between anatomic region and by disease state

A schematic detailing the experimental procedures and designation of the lung anatomical region studies is depicted in Fig. 1. Confirmation of adequate decellularization is shown in Supplemental Fig. 1A and has also been presented in a previous manuscript [14]. For subsequent analyses of GAG content and function, nonsmokers with no history of lung disease and remote smokers were combined into a single group. The total GAG content segregated by region and disease process is depicted in Fig. 2 with raw data

shown in Supplemental Tables 1–3. These results demonstrate similar amounts of total GAGs in bulk lung for all three conditions. However, significantly lower amount of total GAGs was observed in the airway compartment of IPF lungs and a trend towards lower amounts was noted in the distal airway/alveolar-enriched and vascular compartments of lungs from COPD and IPF patients compared to those with normal lungs. Comparisons between regions in each group demonstrated that total GAG amountswere higher in airways compared to other compartments, regardless whether lungs were normal or from patients with either COPD or IPF.

The total content and relative percent composition of the major GAG classes, HS, CS, and HA segregated by region and disease process is depicted in Fig. 3 with raw data shown in Supplemental Tables 1–3. Total HS was significantly lower in the bulk and vasculature groups of IPF lungs compared to normal or COPD lungs with a trend towards lower amounts in airway and alveolar regions (Fig. 3A,B). There was a trend towards lower total HS in all regions of COPD lung compared to normal lungs. Comparisons between regions demonstrated significantly lower total HS in airways of normal and COPD lungs and a trend towards lower amounts in IPF lungs compared to the other regions. The percent HS declined in airways in all groups compared to other regions and vasculature HS percents were lower compared to bulk in normal lungs. In contrast, total CS was higher in the airways compartment compared to bulk and the other compartments in normal lungs with a trend towards decrease in COPD and IPF lungs (Fig. 3C). However, there was more variability of total CS in airways compared to the other compartments. Comparisons between regions in each group demonstrated that the percent CS was similarly higher in airways in normal and COPD lungs as well as in IPF lungs (Fig. 3D). Total HA was comparably higher in the airways of normal, COPD, and IPF lungs compared to other regions. The airways compartment of IPF has the highest HA percent compared to that of normal and COPD lungs (Fig. 3E,F).

3.2. HS and CS disaccharide composition varies between anatomic regions

The comparative and relative HS and CS disaccharide compositions classified by region are depicted in Fig. 4. The acronyms associated with each HS and CS composition are defined in **Supplemental Table 4** and raw data for each individual specimen is displayed in **Supplemental Tables 5–10**. The t-test statistics were

Acta Biomaterialia 168 (2023) 388-399

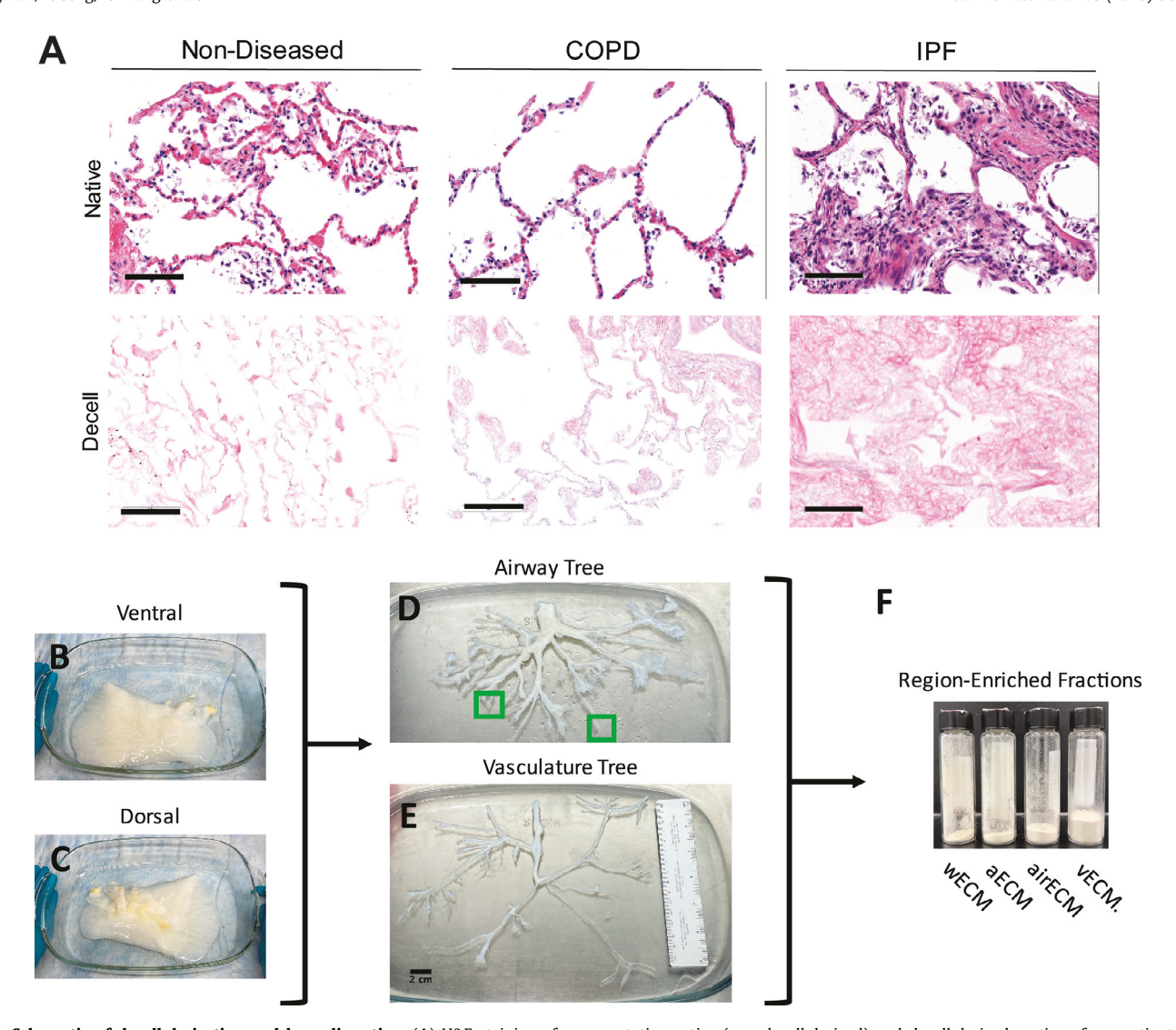


Fig. 1. Schematic of decellularization and lung dissection. (A) H&E staining of representative native (non-decellularized) and decellularized sections from patients with non/remote smokers with no history of lung disease (non-diseased), COPD, or IPF. Sca1e bar = 10μm. (B-F) Stepwise procedure of dissecting decellularized lungs to obtain ECM powder from each anatomical lung region. Whole decellularized lungs (B,C) were dissected to isolate airway and vasculature trees (D,E) and alveolar-enriched regions were obtained from the distal tips of the airway trees (D, green boxes). Isolated lungs regions were subsequently lyophilized and milled into a fine powder for downstream analysis (F). wECM = whole lung ECM, aECM = alveolar-enriched ECM, airECM = airway ECM, vECM = vascular ECM.

performed by using the average values of the specimens from the same region and disease state. A significant lower amount of the HS-associated non-sulfated disaccharide, Δ UA-GlcNAc (0S), was observed in airways when compared to the other regions, as shown in Fig. 4C. Conversely, both the HS and CS were associated with higher amounts of 6-sulfated disaccharides, while the CS-associated 4-sulfated disaccharide, Δ UA-GalNAc-4S (4S), was lower in airways. Additionally, the average percentage of HS TriS disaccharides was increased in IPF lungs when the average values from the four regions were included in the t-test (not shown in the figure).

3.3. Disaccharide composition of purified HS and CS for SPR chip preparation

The disaccharide composition of the purified HS and CS used in the SPR assay was analyzed and depicted in Fig. 5. In bulk lungs, the proportion of highly sulfated HS building blocks (TriS, NS6S, NS2S) followed a pattern of normal > COPD > IPF. Conversely, the proportion of non-sulfated HS followed a pattern of IPF > COPD > normal lung. Additionally, IPF lungs had a higher proportion of

6-O-sulfated CS compared to both normal and COPD lungs. The sulfation level of the purified HS from various disease-state lungs exhibited a different pattern compared to that seen in the original, unprocessed specimens. The purified HS from IPF lungs had a lower proportion of sulfated dp2, which will be further discussed in the discussion section.

3.4. Decellularized IPF lung ECM GAGs are less able to bind matrix-associated growth factor binding compared to normal or COPD lungs

Matrix-associated growth factor binding to and activation by GAGs is dependent on the GAG chain disaccharide composition. We have previously found that decellularization decreases the ability of GAGs remaining in the ECM to bind matrix-associated growth factors FGF2 and TGF β [2]. As specific GAGs were decreased and/or proportionally changed depending on anatomical region or on disease state, it was important to further determine whether their ability to bind matrix-associated growth factors was altered, particularly in disease. Comparative SPR studies were therefore performed in lungs obtained from normal/former smoker, COPD, and

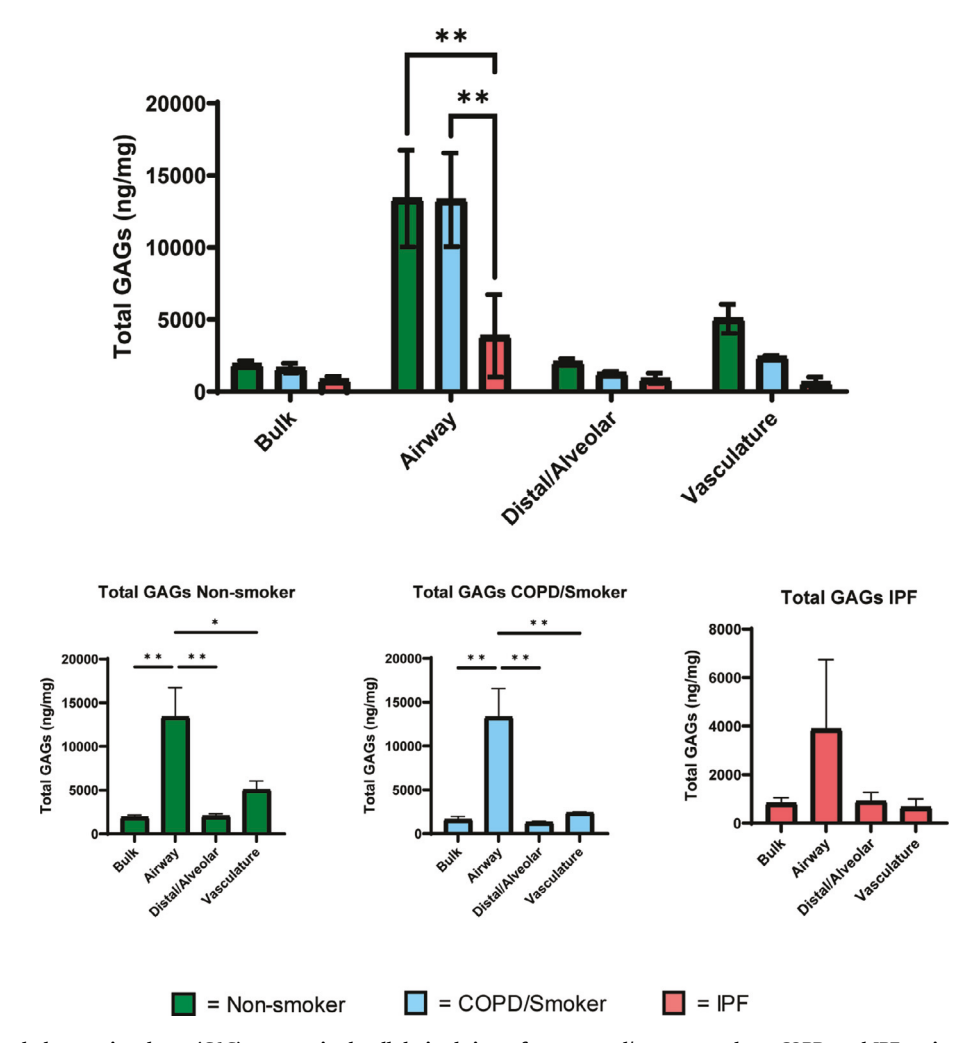


Fig. 2. Comparison of total glycosaminoglycan (GAG) amount in decellularized tissue from normal/remote-smokers, COPD, and IPF patients. (A) Total amount of GAGs (ng/mL) from each lung region and condition analyzed by two-way ANOVA with Tukey's multiple comparisons test, **=p<0.01. (B) Total amount of GAGs from individual lung conditions analyzed by one-way ANOVA with Tukey's multiple comparisons test, *=p<0.05, **=p<0.01. Results are obtained from 6 individual non-smoker/remote smoker, 3 COPD, and 3 IPF lung samples.

Table 1B Additional lungs utilized for SPR analyses.

| Patient ID | Lung Designation | Age | Sex | Pulmonary History | Smoking History |
|------------|------------------|-----|-----|------------------------------------|---|
| ND7 | Non-diseased | 54 | M | None | Ex-smoker, quit 34 years prior to death |
| ND8 | Non-diseased | 41 | M | None | Lifelong non-smoker |
| COPD4 | COPD | 42 | M | COPD | Ex-smoker, quit 4 years prior to death |
| COPD5 | COPD | 65 | M | Centrilobular and distal emphysema | Current smoker |

IPF patients to assess whether binding of these growth factors differed by disease. For these studies, only bulk lung samples (information of the normal and COPD specimens was provided in Table 1B, IPF group used the bulk specimens from Table 1 A) were utilized as the amount of available regional materials was limiting. Sensorgrams of cytokine-GAG interaction are shown in Fig. 6. A 1:1 binding model was applied to fitting the curves and the kinetics of cytokine-GAG interaction are shown in Table 2A, B. Heparin was used as reference for both FGF2 and TGF β 1 binding.

In summary, the HS has a higher affinity for FGF2 than for TGF- β 1, which aligns with the characteristics of heparin (as seen in Table 2 A, B). Kinetic analysis of FGF2 interactions with IPF GAGs showed that IPF HS and CS have a lower affinity (k_a) but a higher rate of dissociation (k_d) and overall dissociation constant (K_D) compared to HS and CS from normal and COPD lungs. This suggests that compared to HS and CS from normal and COPD lungs, HS and

CS from IPF lungs bind to FGF2 more slowly but disassociate faster, leading to a weaker overall interaction.

Top of Form

In contrast to the FGF2 interactions, the overall affinity between TGF- $\beta1$ and lung HS is weaker than that between TGF- $\beta1$ and lung CS. The binding of TGF- $\beta1$ to HS was increased in IPF lungs compared to normal and COPD lungs, while binding to CS was comparable across all three groups. Although the IPF CS demonstrated a higher rate of dissociation (k_d) in TGF- $\beta1$ binding compared to the other two groups, the overall dissociation constant (K_D) did not show a significant increase due to the increased affinity (k_a) value.

Overall, the kinetic data shows that CS from IPF lungs has a faster rate of dissociation from both FGF2 and TGF- β 1 compared to normal or COPD lungs. This means that the interaction time between IPF CS and cytokines is short. The differences in GAG composition between normal and diseased lungs may play a signifi-

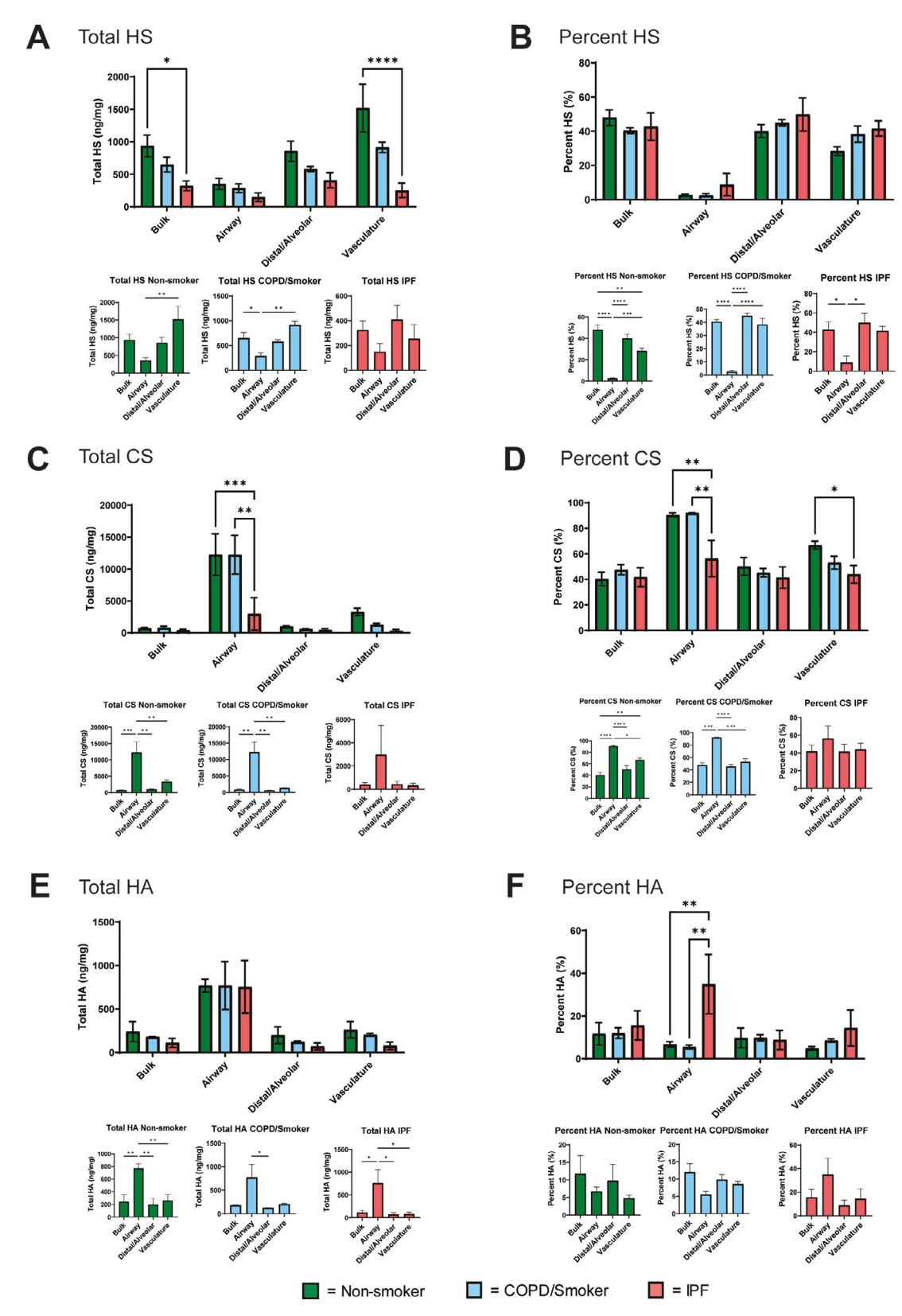


Fig. 3. Comparative quantification and relative percent composition of heparan sulfate (HS), chondroitin sulfate/dermatan sulfate (CS/DS), and hyaluronic acid (HA) varies per region and by disease state. (A) Total HS; (B) Percent HS; (C) Total CS/DS; (D) Percent CS/DS; (E) Total HA; (F) Percent HA. Parallel analysis of both individual lung regions and conditions were performed using two-way ANOVA with Tukey's multiple comparisons test, *= p < 0.05, **= p < 0.001, **** = p < 0.001, *** = p < 0.001, **** = p < 0.001, *** = p < 0.001

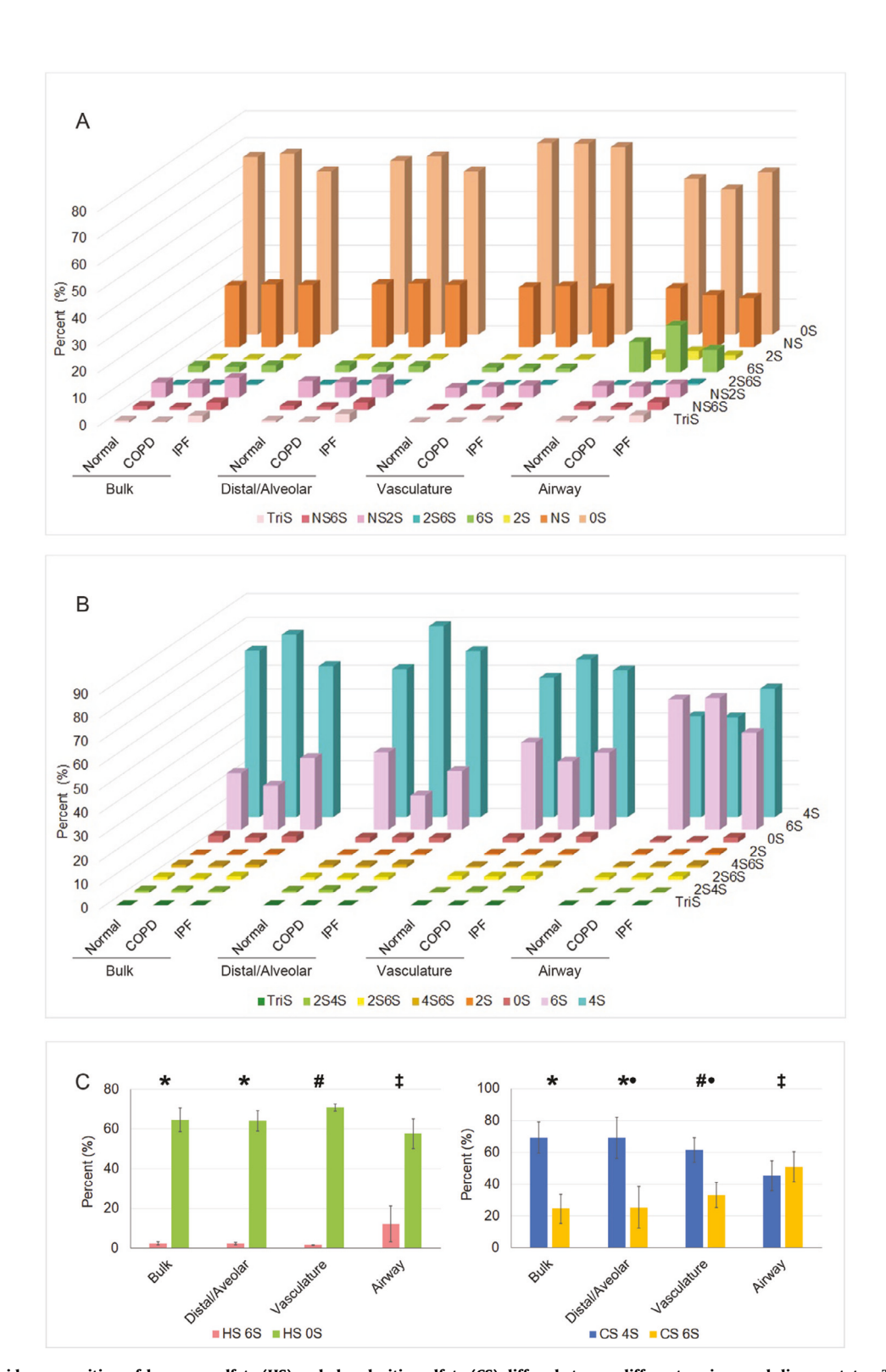


Fig. 4. The disaccharide composition of heparan sulfate (HS) and chondroitin sulfate (CS) differs between different regions and disease states. The disaccharide compositions of both HS and CS are shown in panels (A) and (B), respectively. Panel (C) shows the percent differences in the proportion of 6-sulfated (6S) and non-sulfated (0S) HS disaccharides (left) and 4-sulfated (4S) and 6-sulfated (6S) CS disaccharides (right) between the different regions. The data was analyzed using a two-tailed t-test with unequal variance, and the results showed that there were no significant differences between groups that were marked with the same or partially same symbol (p<0.05). For example, the proportion of 4S and 6S in CS from the Distal region was found to be not significantly different from that of the Bulk or Vascular regions, but showed significant differences from that of the Airway region.

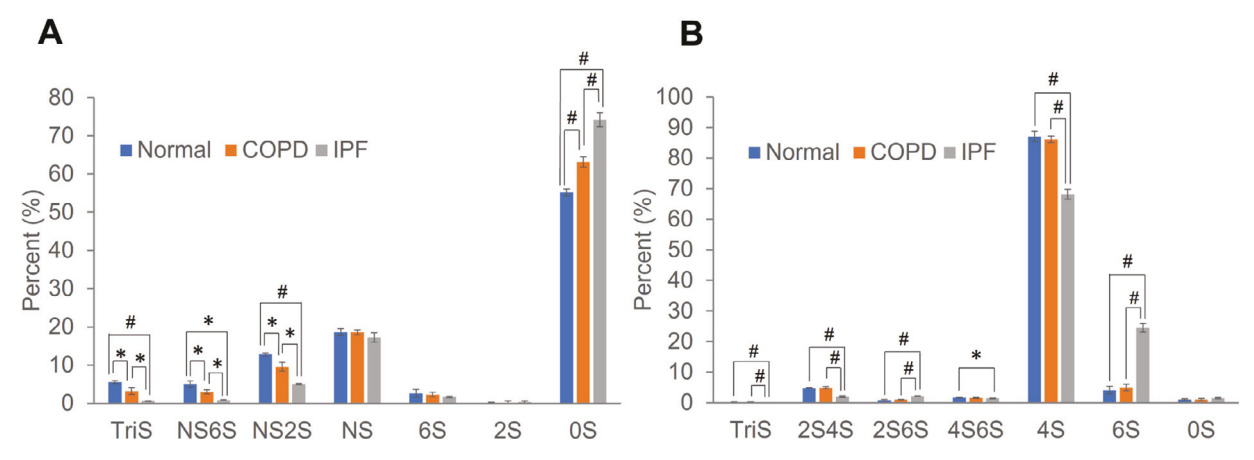


Fig. 5. The disaccharide composition of purified heparan sulfate (HS) and chondroitin sulfate (CS) used in the SPR assay. The HS and CS from normal and COPD subjects were obtained from pooled bulk specimens, the information of which is provided in Table 1B. The IPF HS and CS were recovered from pooled bulk specimens listed in Table 1A. Panel A of the figure shows the disaccharide composition of the purified HS, while panel B displays the disaccharide composition of the purified CS. The difference between the disaccharide compositions of the different groups was tested using a two-tailed t-test with unequal variance. The results showed that there were significant differences between some groups, indicated by asterisks (*) for p values between 0.01 and 0.05, and hash symbols (#) for p values less than 0.01.

Table 2AKinetic data of FGF2- lung GAG interactions (1:1 binding model)*.

| Interaction | k _a (1/MS) | k _d (1/S) | $K_D(M)$ |
|--|---|---|---|
| FGF2-HS normal FGF2-HS COPD FGF2-HS IPF FGF2-CS normal FGF2-CS COPD FGF2-CS IPF | $2.9 \times 10^4 \ (\pm 5.0 \times 10^2)$ $2.3 \times 10^4 \ (\pm 3.9 \times 10^2)$ $6.7 \times 10^3 \ (\pm 1.2 \times 10^2)$ $9.7 \times 10^3 \ (\pm 1.1 \times 10^2)$ $9.7 \times 10^3 \ (\pm 0.6 \times 10^2)$ $3.1 \times 10^3 \ (\pm 0.5 \times 10^2)$ | $\begin{array}{c} 1.9 \times 10^{-3} \ (\pm 3.9 \times 10^{-5}) \\ 7.2 \times 10^{-4} \ (\pm 3.8 \times 10^{-5}) \\ 3.5 \times 10^{-3} \ (\pm 4.1 \times 10^{-5}) \\ 5.8 \times 10^{-3} \ (\pm 3.5 \times 10^{-5}) \\ 6.4 \times 10^{-3} \ (\pm 2.0 \times 10^{-5}) \\ 1.2 \times 10^{-2} \ (\pm 7.0 \times 10^{-5}) \end{array}$ | 6.7×10^{-8} 3.2×10^{-8} 5.2×10^{-7} 6.0×10^{-7} 6.6×10^{-7} 3.7×10^{-6} |
| FGF2-heparin | $9.9{\times}10^5~(\pm~2.7{\times}10^4)$ | $8.2 \times~10^{-5}~(\pm~1.9 \times 10^{-6})$ | 8.3×10^{-11} |

Table 2B Kinetic data of TGF- β 1 - lung GAG interactions (1:1 binding model)*.

| Interaction | k _a (1/MS) | k _d (1/S) | $K_D(M)$ |
|---|---|--|--|
| TGF- β 1 -HS normal TGF- β 1 -HS COPD TGF- β 1 -HS IPF TGF- β 1 -CS normal TGF- β 1 -CS COPD TGF- β 1 -CS IPF TGF- β 1 -heparin | $4.3 \times 10^3 \ (\pm \ 2.0 \times 10^2)$ $3.4 \times 10^3 \ (\pm \ 1.2 \times 10^2)$ $1.8 \times 10^4 \ (\pm \ 1.4 \times 10^3)$ $8.5 \times 10^4 \ (\pm \ 2.0 \times 10^2)$ $1.4 \times 10^5 \ (\pm \ 2.5 \times 10^3)$ $3.0 \times 10^5 \ (\pm \ 1.9 \times 10^4)$ $1.9 \times 10^6 \ (\pm \ 2.6 \times 10^4)$ | $\begin{array}{c} 0.10 \ (\pm 1.2 \times 10^{-3}) \\ 8.5 \times 10^{-2} \ (\pm \ 7.5 \times 10^{-4}) \\ 0.14 \ (\pm 9.5 \times 10^{-3}) \\ 6.7 \times 10^{-2} \ (\pm \ 1.5 \times 10^{-4}) \\ 5.8 \times 10^{-2} \ (\pm \ 3.3 \times 10^{-4}) \\ 0.16 \ (\pm 7.4 \times 10^{-3}) \\ 3.2 \times \ 10^{-2} \ (\pm 3.2 \times 10^{-4}) \end{array}$ | 2.4×10^{-5} 2.5×10^{-5} 8.0×10^{-6} 7.9×10^{-7} 4.1×10^{-7} 5.4×10^{-7} 1.7×10^{-8} |

^{*}The data with (\pm) in parentheses are the standard deviations (SD) from fitting of five to seven different concentration of FGF2 or TGF- β 1 injections.

cant role in affecting their cytokine binding properties. It's worth noting that the purified HS from IPF lungs has a lower sulfation level, while the CS has a higher sulfation level at the 6-O position, which may contribute to the faster dissociation of cytokines from IPF GAGs.

4. Discussion

GAGs are increasingly recognized to play important roles in normal lung homeostasis and in lung disease pathogenesis (2,3,11-13). However, there remains only limited knowledge about the functional roles of individual GAGs and their disaccharide compositions in specific lung diseases (11-13). Further available data has mostly evaluated GAG composition in intact lungs in which cell-associated GAGs can obscure the roles and functions of ECM-associated GAGs. To better understand the role of ECM in lung homeostasis and disease, decellularized lungs and materials derived from them are increasingly utilized in lung regenerative medicine and engineering applications. However, while total GAGs have long been recognized to decrease after decellularization, to date there is only limited assessment of individual GAG composition and potential correlative

functional effects in the decellularized scaffolds [2]. Further, analyses to date have been done utilizing whole lung samples and potential differences between GAG composition in anatomic compartments such as airways, vascular, and alveoli are less well characterized. This also includes limited assessment in diseased lungs where it has been previously been demonstrated that decellularized COPD as well as IPF lungs scaffolds differently affects behavior of inoculated cells compared to decellularized non-diseased lung matrices [16,21–23]. However, the mechanisms for those effects still need to be elucidated.

Qualitative decrease in total lung GAG content with decellularization has previously been demonstrated utilizing Alcian blue histologic staining or by quantification of sulfated GAGs in decellularized lung homogenates [15,16,20]. We had further demonstrated quantitative decreases in the in total GAGs, the major GAG classes HS, CS/DS, and HA, and in selected GAG disaccharides and sulfation patterns following decellularization of whole (bulk) normal and COPD lungs [2]. No influence of smoking status, disease state, age, gender, or time to autopsy before tissue curation and subsequent decellularization was observed in that study although the number of samples was limited. Further, GAGs isolated from the decellu-

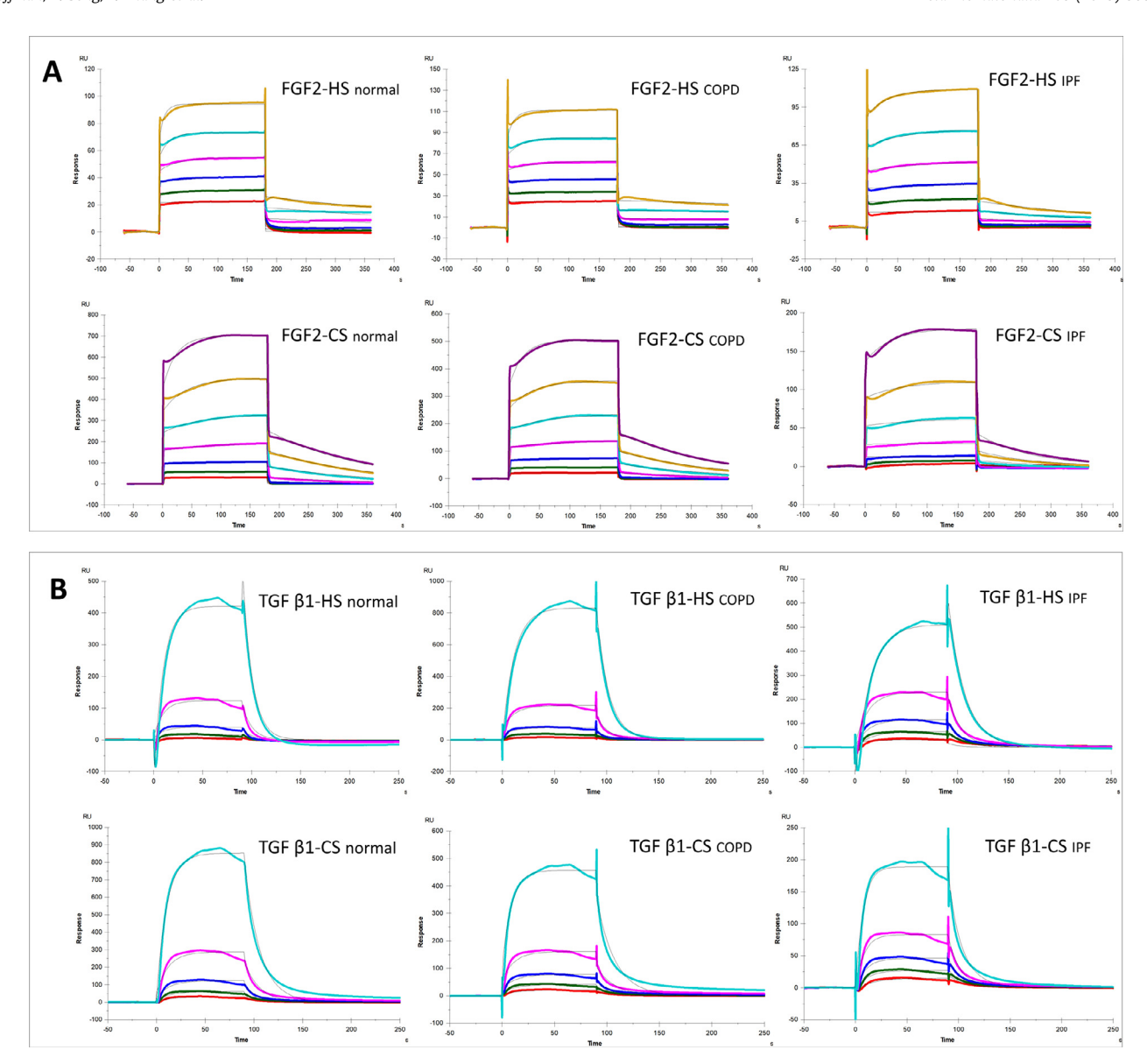


Fig. 6. SPR sensorgrams of cytokines interaction with purified heparan sulfate (HS) and chondroitin sulfate (CS) from pooled bulk samples of normal, COPD and IPF specimens. A. FGF2 interaction with HS and CS. B. TGF β1 interaction with HS and CS. Concentrations of FGF2 in HS sensorgrams are (from top to bottom) 4000 (yellow), 2000 (light blue), 1000 (magenta), 500 (blue), 250 (green) and 125 nM (red), respectively. Concentrations of FGF2 in CS sensorgrams are (from top to bottom) 4000 (purple), 2000 (yellow), 1000 (light blue), 500 (magenta), 250 (blue), 125 (green) and 62.5 nM (red), respectively. Concentrations of TGF β1 in HS sensorgrams are (from top to bottom) 800 (light blue), 400 (magenta), 200 (blue), 100 (green), and 50 (red) nM, respectively. Concentrations of TGF β1 in CS sensorgrams are (from top to bottom) 400, 200, 100, 50, and 25 nM, respectively using the same color scheme. The black curves are fitting curves using 1:1 binding models from Biacore T200 Evaluation Software 3.2.

larized normal whole lungs were less able to bind key matrix-associated growth factors, TGF β 1, FGF2, and hepatocyte growth factor (HGF), each of which plays significant roles in cell lung behaviors, [9,10,24–28]. This provided strong and unique evidence that GAGs are both selectively depleted and functionally altered in decellularized human lungs and materials derived from them.

We have now found differential GAG content between anatomic compartments in both normal and diseased decellularized lungs and also in the different compartments when compared between normal and diseased lungs. Notably, major differences were noted in the airways compared to the other compartments with increased total and percent GAGs, increased CS, and decreased HS. In part this may reflects the cartilaginous components of the airways samples studied as cartilage is relatively enriched in CS [29,30]. We did not distinguish between large and medium-sized airways and suspect that more detailed analysis of non-cartilaginous medium-sized and smaller airways may have changed the total amount and

relative GAG proportions. A further observation is that total HS was reduced in both the bulk and vascular compartments of IPF lungs. This observation contrasts with that of Westergren-Thorsson and colleagues who found that the total amount of HS, CS/DS and HA was increased in distal (sub-pleural) regions of IPF lungs [12]. However, these were intact rather than decellularized lungs and contain contributions from cell-associated GAGs.

We had previously observed disproportionate changes in HS and CS disaccharide composition following decellularization of bulk normal and COPD lungs [2] and now have further found differences both between regions and between normal and diseased lungs. Significant reduction of HS-associated non-sulfated disaccharide Δ UA-GlcNAc (0S) was observed in airways compared to the other regions. Conversely, both HS and CS associated 6-sulfated disaccharide increased whereas the CS associated 4-sulfated disaccharide Δ UA-GalNAc-4S (4S) was decreased compared to the other regions (Fig. 4). The IPF specimen showed a general increased HS

E. Hoffman, Y. Song, F. Zhang et al. Acta Biomaterialia 168 (2023) 388–399

TriS percentage compared to normal and COPD lungs. In comparison to our findings in decellularized IPF lungs, Westergren-Thorsson and colleagues had found a relative increase in total sulfation of HS due to increment of 2-O, 6-O and N-sulfation and a higher proportion of sulfation in CS/DS in intact IPF lungs [12]. Interestingly, immunohistologic analyses demonstrated that highly sulfated HS was located in the border zone between denser areas and more normal looking alveolar parenchyma in basement membranes of blood vessels and airways. However, these reflected both ECM and cell-associated changes in GAG content.

For the purified GAGs used to prepare SPR chips, the disaccharide composition was found to have different patterns, with the HS from IPF lungs being less sulfated compared to normal and COPD lungs. This difference could be due to a potential loss of highly sulfated HS during the acetone precipitation and anion exchange purification procedure. Our research found that cytokines exhibit a higher affinity for HS with a higher proportion of sulfated disaccharides. Thus, it is possible that the IPF specimens may have originally contained some highly sulfated HS that could compensate for the reduced affinity of cytokines with the less-sulfated HS found in the ECM.

Despite these possible limitations, the observations from the SPR assays have potential functional ramifications as the different side chains have different roles in binding matrix-associated growth factors. For instance, binding of members of FGF ligand family to their receptors, including FGF1 and FGF2 to FGFR1 and FGFR2, has previously been shown to require N-, 2-0, and 6-0 sulfated HS [8,9]. The bioactivity of TGF β 1 has also been demonstrated to be dependent on the degree of sulfation of HS polymers but it is not known if this interaction is specific or rather a matter of non-specific electrostatic interactions [10]. Accordingly, we found that compared to HS and CS from normal and COPD lungs, HS and CS from IPF lungs bound to FGF2 more slowly but disassociated faster indicating a lower overall strength of the interaction. We also observed that CS from IPF lungs disassociated faster from both FGF2 and TGF β 1 than from normal or COPD lungs. This indicates that the interaction-existing time is short for IPF CS when binding to cytokines. Notably, the purified HS from IPF lungs is less sulfated and the CS is more sulfated at 6-0 position, which may be the reason for the cytokines to disassociate faster from IPF GAGs. Overall, this data supports the concept that differences in GAG composition between decellularized normal and diseased lungs is a major factor in affecting their cytokine binding features [2,5,13].

It is important to note that dermatan sulfate (DS), also known as chondroitin sulfate B or CS-B, is another glycosaminoglycan found in lung tissue that cannot be differentiated from chondroitin sulfate (CS) using disaccharide analysis. Therefore, it is possible that the CS component tested in our study contained some DS. Although CS is not considered a key regulator of FGF2 activity, it demonstrated notable binding to FGF2 in our SPR assay. This binding may have been contributed by the presence of dermatan sulfate. Nonetheless, our hypothesis is that the binding of CS (or DS) and FGF2 is mainly due to unspecified electrostatic interaction.

As indicated by the disaccharide composition analysis, HS has over 60% of nonsulfated disaccharides, whereas CS has less than 3% of nonsulfated disaccharides. Consequently, CS may more easily attract proteins due to its higher negatively charged property. However, the SPR data showed that the binding of CS to FGF2 had lower k_a (slow association) and higher k_d (fast dissociation) compared to their HS counterpart. The binding strength of CS to FGF2, as reflected by K_D , was 7-20 times lower than that of their HS counterpart. Based on these results, we hypothesize that CS (may contain DS) interacts with FGF2 in an unspecific binding manner, caused by electrostatic interaction.

There are several caveats to the current observations. The results obtained are specific for the TritonX-100, and sodium deoxy-

cholate detergent-based decellularization protocol utilized. Other protocols with different detergents or physical methods such as freeze-thawing may yield different results. Different concentrations of or incubation times with the same detergents might also result in different results. We agree that a comprehensive study of the methodology of decellularization is crucial for advancing the field of organ transplantation. Future studies should include a time course analysis and comparative studies with different methods.

We also acknowledge the limitations in clinical and pathologic characterizations of the lungs utilized as well as batch-to-batch and individual variations among different samples although these tended to be small within each clinical category. We acknowledge that classification of the lungs into populations of normal (nonsmoker or ex-smoker with no diagnosed lung disease), COPD (with or without active smoking at time of death), or IPF. is an imperfect categorization as both normal and diseased lungs can exhibit heterogeneity in both structure and function. Larger scale studies will be necessary to confirm and further explore the observed results. Nonetheless, there was good overall correlation between findings in each study group with generally small variability in the study outcomes. Further, the lungs utilized tended to be from older individuals as reflective of the demographics of lungs available through the University of Vermont autopsy service. AsGAG content and sulfation patterns can change with age [31,32], future studies will also further explore lungs from younger individuals. With respect to the anatomic compartments assessed, we did not separate pulmonary arterial and venous tissues and future studies will need to assess these individually as well to further assess GAG compositions in large vs medium-sized vs smaller airways and vascular regions.

5. Conclusion

Our results demonstrate that the composition and function of GAGs remaining in decellularized lungs varies between different anatomic compartments of the lung as well as differing in diseased lungs. There is a potential correlation between the HS and CS disaccharide composition and their ability to bind and release FGF2 and $TGF\beta$ that is particularly altered in IPF lungs. These observations provide further information for understanding functional roles of ECM GAGs in lung function and disease.

Declaration of Competing Interest

This manuscript has not been published and is not under consideration for publication elsewhere. We have no conflicts of interest to disclose.

Acknowledgements

The authors thank the UVM Autopsy Services and also Robert Pouliot PhD and Juan Uriarte PhD for help with the decellularization of the lung tissue.

This work was supported by the National Institutes of Health, RO1 HL12714401, 2014 (DJW); the Cystic Fibrosis Foundation (WEISS18P0, DJW); NHBLI Lung Biology Training grant T32 HL076122, 2016 (RAP); S10OD028523 (FZ and RJL), Al156573 (FZ and RJL), and the National Science Foundation GlycoMIP DMR 1933525 (FZ and RJL).

Supplementary materials

Supplementary material associated with this article can be found, in the online version, at doi:10.1016/j.actbio.2023.06.043.

References

- [1] L.E. Niklason, Understanding the extracellular matrix to enhance stem cell-based tissue regeneration, Cell Stem Cell 22 (2018) 302-305.
- [2] F.E. Uhl, F. Zhang, R.A. Pouliot, J.J. Uriarte, S. Rolandsson Enes, X. Han, Y. Ouyang, K. Xia, G. Westergren-Thorsson, A. Malmström, O. Hallgren, R.J. Linhardt, D.J. Weiss, Functional role of glycosaminoglycans in decellularized lung extracellular matrix, Acta Biomater. 102 (2020) 231–246.
- [3] Y. Zhou, J.C. Horowitz, A. Naba, N. Ambalavanan, K. Atabai, J. Balestrini, P.B. Bitterman, R.A. Corley, B. Ding, A.J. Engler, K.C. Hansen, J.S. Hagood, F. Kheradman, Q.S. Lin, E. Neptune, L. Niklason, L.A. Ortiz, W.C. Parks, D.J. Tschumperlin, E.S. White, H.A. Chapman, V.J. Thannickal, Extracellular matrix in lung development, homeostasis and disease, Matrix Biol. 73 (2018) 77–104.
- [4] R.J. Linhardt, T. Toida, Role of glycosaminoglycans in cellular communication, Acc. Chem. Res. 37 (2004) 431–438.
- [5] D. Soares da Costa, R.L. Reis, I. Pashkuleva, Sulfation of glycosaminoglycans and its implications in human health and disorders, Annu. Rev. Biomed. Eng. 19 (2017) 1–26.
- [6] E. Sterner, L. Meli, S.J. Kwon, J.S. Dordick, R.J. Linhardt, FGF-FGFR signaling mediated through glycosaminoglycans in microtiter plate and cell-based microarray platforms, Biochemistry 52 (2013) 9009–9019.
- [7] U. Lindahl, J. Couchman, K. Kimata, J.D. Esko, in: Proteoglycans and Sulfated Glycosaminoglycans, Cold Spring Harbor Laboratory Press, New York, 2015, pp. 207–221. in: A. Varki, R.D. Cummings, J.D. Esko, P. Stanley, G.W. Hart, M. Aebi, A.G. Darvill, T. Kinoshita, N.H. Packer, J.H. Prestegard, R.L. Schnaar, P.H. Seeberger (Eds.).
- [8] C. Settembre, E. Arteaga-Solis, M.D. McKee, R. de Pablo, Q. Al Awqati, A. Ballabio, G. Karsenty, Proteoglycan desulfation determines the efficiency of chondrocyte autophagy and the extent of FGF signaling during endochondral ossification, Genes Dev. 22 (2008) 2645–2650.
- [9] A.K. Powell, D.G. Fernig, J.E. Turnbull, Fibroblast growth factor receptors 1 and 2 interact differently with heparin/heparan sulfate. Implications for dynamic assembly of a ternary signaling complex, J. Biol. Chem. 277 (2002) 28554–28563.
- [10] L. Koehler, S. Samsonov, S. Rother, S. Vogel, S. Kohling, S. Moeller, M. Schnabelrauch, J. Rademann, U. Hempel, M.T. Pisabarro, D. Scharnweber, V. Hintze, Sulfated hyaluronan derivatives modulate TGF-beta1: receptor complex formation: possible consequences for TGF-beta1 signaling, Sci. Rep. 7 (2017) 1210.
- [11] G. Burgstaller, B. Oehrle, M. Gerckens, E.S. White, H.B. Schiller, O. Eickelberg, The instructive extracellular matrix of the lung: basic composition and alterations in chronic lung disease, Eur. Respir. J. 50 (2017) 1601–1605.
- [12] G. Westergren-Thorsson, U. Hedstrom, A. Nybom, E. Tykesson, E. Ahrman, M. Hornfelt, M. Maccarana, T.H. van Kuppevelt, G. Dellgren, M. Wildt, X.H. Zhou, L. Eriksson, L. Bjermer, O. Hallgren, Increased deposition of glycosaminoglycans and altered structure of heparan sulfate in idiopathic pulmonary fibrosis, Int. J. Biochem. Cell Biol. 83 (2017) 27–38.
- [13] S. Shojaie, L. Ermini, C. Ackerley, J. Wang, S. Chin, B. Yeganeh, M. Bilodeau, M. Sambi, I. Rogers, J. Rossant, C.E. Bear, M. Post, Acellular lung scaffolds direct differentiation of endoderm to functional airway epithelial cells: requirement of matrix-bound HS proteoglycans, Stem Cell Rep. 4 (2015) 419–430.
- [14] E.T. Hoffman, F.E. Uhl, L. Asarian, B. Deng, C. Becker, J.J. Uriarte, I. Downs, B. Young, D.J. Weiss, Regional and disease specific human lung extracellular matrix composition, Biomaterials 293 (2023) 121960.
- [15] F.W. Uhl, D.E. Wagner, D.J. Weiss, Preparation of decellularized lung matrices for cell culture and protein analysis in fibrosis: methods and protocols, Methods Mol. Biol. 1627 (2017) 253–283.
- [16] D.E. Wagner, N.R. Bonenfant, C.S. Parsons, D. Sokocevic, E.M. Brooks, Z.D. Borg, M.J. Lathrop, J.D. Wallis, A.B. Daly, Y.W. Lam, B. Deng, M.J. DeSarno, T. Ashikaga, R. Loi, D.J. Weiss, Comparative decellularization and recellularization of normal versus emphysematous human lungs, Biomaterials 35 (2014) 3281–3297.

- [17] N. Volpi, F. Galeotti, B. Yang, R.J. Lindhardt, Analysis of glycosaminoglycan-derived, precolumn, 2-aminoacridone-labeled disaccharides with LC-fluorescence and LC-MS detection, Nat. Protoc. 9 (2014) 541–558.
- [18] G. Li, L. Li, F. Tian, L. Zhang, C. Xue, R.J. Lindhardt, Glycosaminoglycanomics of cultured cells using a rapid and sensitive LC-MS/MS approach, ACS Chem. Biol. 10 (2015) 1303–1310.
- [19] F. Zhang, K.B. Lee, R.J. Linhardt, SPR biosensor probing the interactions between TIMP-3 and Heparin/GAGs, Biosensors 5 (2015) 500-512 (Basel).
- [20] J.M. Wallis, Z.D. Borg, A.B. Daly, B. Deng, B.A. Ballif, G.B. Allen, D.M. Jaworski, D.J. Weiss, Comparative assessment of detergent-based protocols for mouse lung de-cellularization and re-cellularization, Tissue Eng. Part C Methods 18 (2012) 420–432.
- [21] D. Sokocevic, N.R. Bonenfant, D.E. Wagner, Z.D. Borg, M.J. Lathrop, Y.W. Lam, B. Deng, M.J. Desarno, T. Ashikaga, R. Loi, A.M. Hoffman, D.J. Weiss, The effect of age and emphysematous and fibrotic injury on the re-cellularization of de-cellularized lungs, Biomaterials 34 (2013) 3256–3269.
- [22] A.J. Booth, R. Hadley, A.M. Cornett, A.A. Dreffs, S.A. Matthes, J.L. Tsui, K. Weiss, J.C. Horowitz, V.F. Fiore, T.H. Barker, B.B. Moore, F.J. Martinez, L.E. Niklason, E.S. White, Acellular normal and fibrotic human lung matrices as a culture system for *in vitro* investigation, Am. J. Respir. Crit. Care Med. 186 (2012) 866–876.
- [23] U. Hedstrom, O. Hallgren, L. Oberg, A. DeMicco, O. Vaarala, G. Wester-gren-Thorsson, X. Zhou, Bronchial extracellular matrix from COPD patients induces altered gene expression in repopulated primary human bronchial epithelial cells, Sci. Rep. 8 (2018) 3502.
- [24] V. Schultz, M. Suflita, X. Liu, X. Zhang, Y. Yu, L. Li, D.E. Green, Y. Xu, F. Zhang, P.L. DeAngelis, J. Liu, R.J. Lindhardt, Heparan sulfate domains required for fibroblast growth factor 1 and 2 signaling through fibroblast growth factor receptor 1c, J. Biol. Chem. 292 (2017) 2495–2509.
- [25] E. Sterner, S. Masuko, G. Li, L. Li, D.E. Green, N.J. Otto, Y. Xu, P.L. DeAngelis, J. Liu, J.S. Dordick, R.J. Lindhardt, Fibroblast growth factor-based signaling through synthetic heparan sulfate blocks copolymers studied using high cell density three-dimensional cell printing, J. Biol. Chem. 289 (2014) 9754–9765.
- [26] K.R. Catlow, J.A. Deakin, Z. Wei, M. Delehedde, D.G. Fernig, E. Gherardi, J.T. Gallagher, M.S. Pavao, M. Lyon, Interactions of hepatocyte growth factor/scatter factor with various glycosaminoglycans reveal an important interplay between the presence of iduronate and sulfate density, J. Biol. Chem. 283 (2008) 5235–5248.
- [27] Y. Ito, K. Correll, J.A. Schiel, J.H. Finigan, R. Prekeris, R.J. Mason, Lung fibroblasts accelerate wound closure in human alveolar epithelial cells through hepatocyte growth factor/c-Met signaling, Am. J. Physiol. Lung Cell. Mol. Physiol. 307 (2014) L94–105.
- [28] M.M. Myerburg, J.D. Latoche, E.E. McKenna, L.P. Stabile, J.S. Siegfried, C.A. Feghali-Bostwick, J.M. Pilewski, Hepatocyte growth factor and other fibroblast secretions modulate the phenotype of human bronchial epithelial cells, Am. J. Physiol. Lung Cell. Mol. Physiol. 292 (2007) L1352–L1360.
- [29] J.P Bali, H. Cousse, E. Neuzil, Biochemical basis of the pharmacologic action of chondroitin sulfates on the osteoarticular system, Semin. Arthritis Rheum. 31 (2001) 58–68.
- [30] P.L. Sannes, K.K. Burch, J. Khosla, K.J. McCarthy, J.R. Couchman, Immunohisto-chemical localization of chondroitin sulfate, chondroitin sulfate proteoglycan, heparan sulfate proteoglycan, entactin, and laminin in basement membranes of postnatal developing and adult rat lungs, Am. J. Respir. Cell Mol. Biol. 8 (1993) 245–251.
- [31] A.M. Hitchcock, K.E. Yates, C.E. Costello, J. Zaia, Comparative glycomics of connective tissue glycosaminoglycans, Proteomics 8 (2008) 1384–1397.
- [32] H.Y. Lee, L. Han, P.J. Roughley, A.J. Grodzinsky, C. Ortiz, Age-related nanos-tructural and nanomechanical changes of individual human cartilage aggrecan monomers and their glycosaminoglycan side chains, J. Struct. Biol. 181 (2013) 264–273.